5.0 CIRCULATION AND OFFSHORE SEDIMENT TRANSPORT DYNAMICS

This section analyzes the physical processes regime of the central east Florida continental shelf and discusses circulation and sediment transport processes to evaluate the potential environmental impact of offshore sand mining. Current and wave processes provide physical mechanisms for moving sediment within the coastal zone of central east Florida. The following discussion documents current and shelf sediment transport processes potentially impacted by sand mining at specific offshore sand borrow sites.

5.1 CURRENTS AND CIRCULATION

Current measurements along the central east Florida shelf were acquired to develop an understanding of shelf circulation processes at proposed offshore borrow sites. These measurements included long-term current meter time series and synoptic spatial surveys at specific offshore shoals for approximately 24-hour periods. Long-term current meter measurements were obtained from previous research programs conducted in the study area. The synoptic observations were obtained specifically for this study and consisted of current profiling from survey vessels at Sand Resource Areas B1 and B2.

5.1.1 Historical Data Analysis

Long-term measurements of shelf currents were evaluated to develop an understanding of the time scales and magnitudes of circulation processes. Several data sets were used for this analysis. These data were obtained in two locations offshore St. Lucie Inlet at inner- and mid-shelf depths. Both data sets were obtained from Dr. Ned Smith of Harbor Branch Oceanographic Institution. There were few other sources of available current meter data for the study region.

Mid-shelf measurements were obtained in 44-m water depth; the sensor was positioned 2 m off the bottom. Data were obtained during two measurement periods: June to November 1977 (137-day record) and March to July 1978 (also 137-day record). A 115-day gap during winter months existed between measurement phases. Data were received as 2-hour averages. Inner shelf measurements, obtained in 10-m water depth near the sea buoy at St. Lucie Inlet, represented current conditions from August to September 1991. Data were received as 20-minute samples, each sample resulting from a 10-minute average at the beginning of the sample window.

Data analyses included statistical sampling, time series analysis including spectral estimates, digital filtering, and tidal harmonic analysis. The analysis goal was to determine significant time scales and amplitudes of observed current variability at potential offshore borrow sites.

5.1.1.1 Description of Observed Currents

Currents were presented as along-shelf and cross-shelf components for the mid-depth station (Figure 5-1). A comparison of these two data sets shows along-shelf currents generally were more variable and stronger than cross-shelf currents. Cross-shelf amplitudes were about ±20 cm/sec, while along-shelf variations approached 50 cm/sec at times. Along-shelf flows were dominated by periodic events (pulses) that persisted for several days. These events were characterized by strong up-shelf (to the north) or down-shelf (to the south) currents. Down-shelf events were observed in October-November 1977 and March-April 1978. Up-shelf events were more common in summer months.

Current observations obtained on the inner shelf near St. Lucie Inlet during late summer 1991 demonstrated similar variability; along-shelf currents were more variable than cross-shelf currents (Figure 5-2). Peak currents approached 50 cm/sec to the north, with sharp flow reversals over time scales of about 1 day. Tidal flow from St. Lucie Inlet may have influenced these data.

The along-shelf dependence of current observations is illustrated in Figure 5-3. The shoreline is oriented approximately north-northwest to south-southeast (340°/160°) at St. Lucie Inlet, and the rose diagrams show a dominance of flow parallel to the coast. While some occurrences of predominantly cross-shelf flow were observed, cross-shelf currents were generally quite weak. Along-shelf currents were most common.

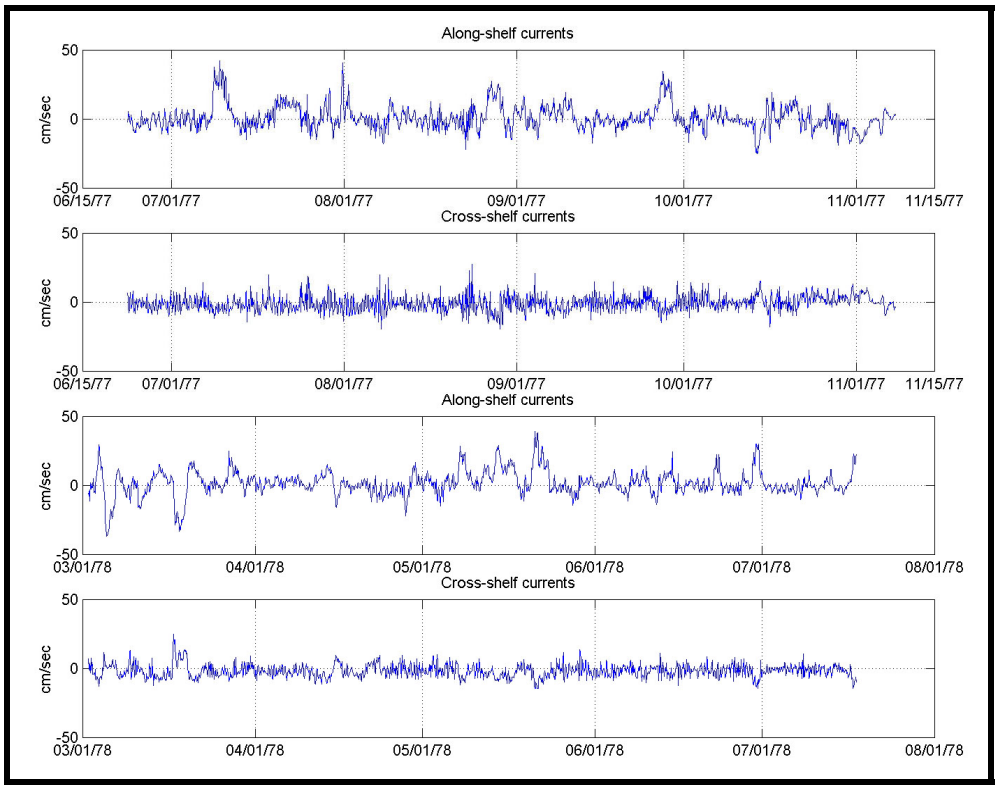

Figure 5-1. Time series of mid-shelf current observations offshore St. Lucie Inlet. Top two plots represent along-shelf and cross-shelf components of near-bottom currents in 44-m water depth obtained June through November 1977. Bottom two plots represent the time period March through July 1978. Data courtesy of Dr. Ned Smith, Harbor Branch Oceanographic Institution.

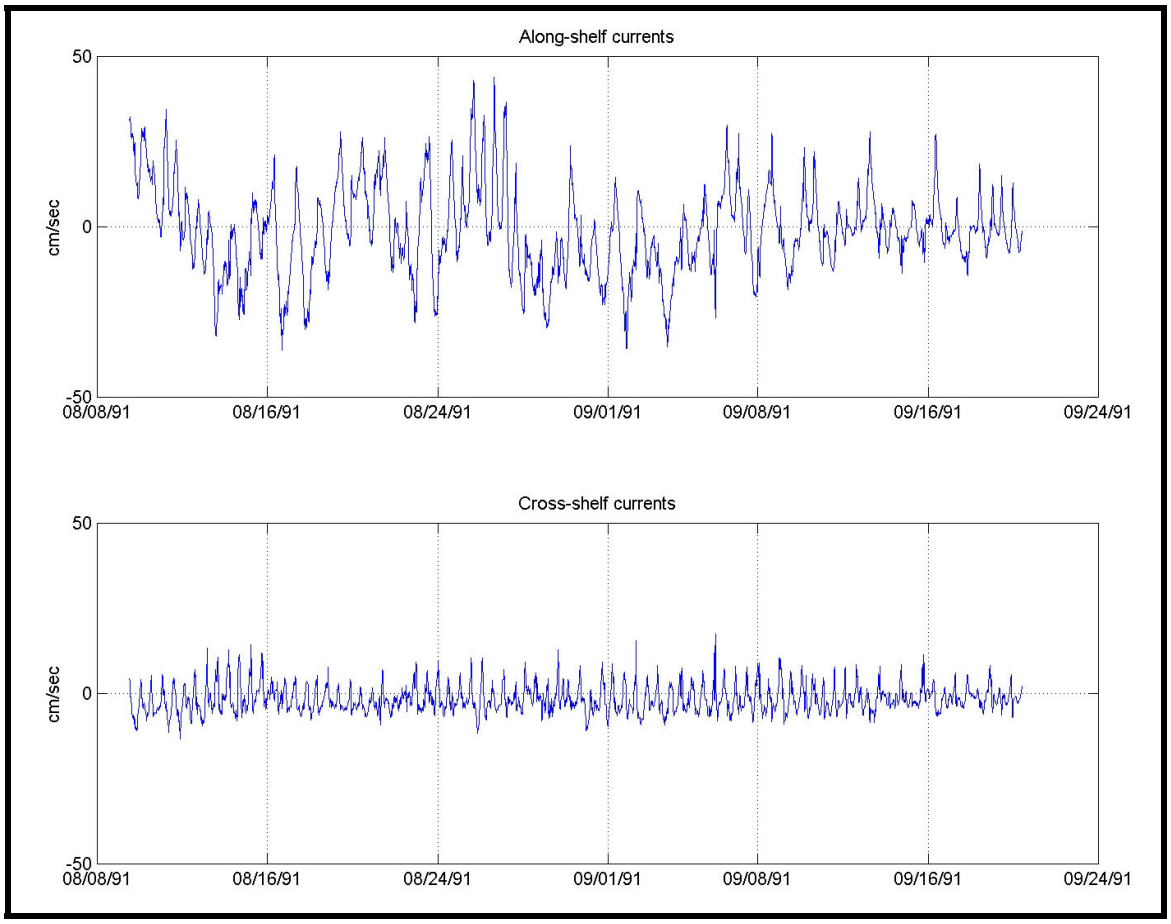

Figure 5-2. Inner shelf current meter observations obtained near St. Lucie Inlet, August 9 to September 20, 1991. Top plot represents the along-shelf current component; bottom plot represents the cross-shelf component. Data courtesy of Dr. Ned Smith, Harbor Branch Oceanographic Institution.

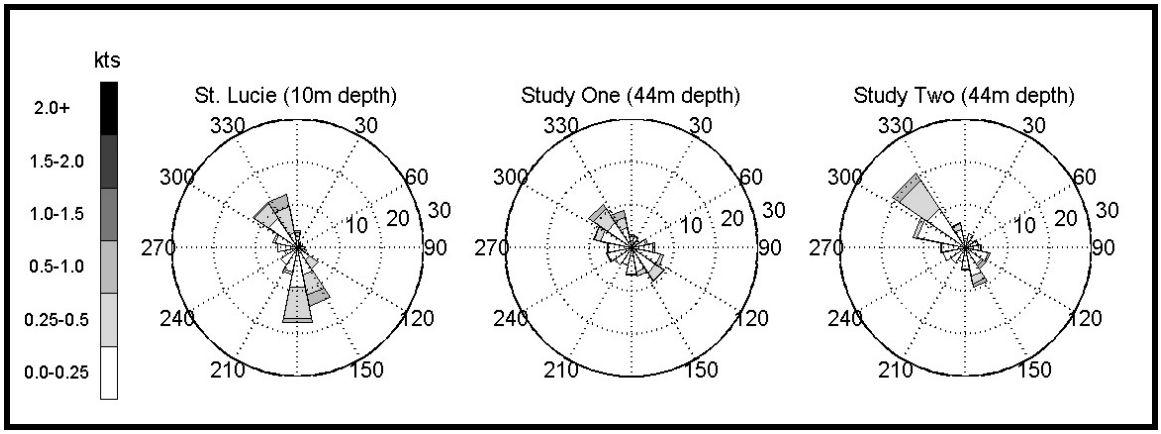

Figure 5-3. Summary of current meter observations presented in Figures 5-1 and 5-2. These graphical presentations show the dominance of along-shelf flow.

Table 5-1 presents summary statistics for the current meter data sets. The magnitude of maximum currents (i.e., positive or northward currents) were always greater than the magnitude of down-shelf currents (i.e., negative or southward currents). Mean along-shelf flows were slightly positive but near zero due to up- and down-shelf current reversals. Mean cross-shelf currents were negative (i.e., onshore). Peak bottom currents of 42 cm/sec were measured on the mid-shelf; these currents were directed northerly (331 deg). Peak current speeds of 44 cm/sec were observed on the inner shelf, oriented toward 340 deg.

Table 5-1. Statistics of current observations.

Location	Along-Shelf Component (cm/sec)				Cross-Shelf Component (cm/sec)			
	Mean	Max	Min	Variance	Mean	Max	Min	Variance
Mid-shelf (44 m) (Jun-Nov 1977)	1.2	42.2	-25.1	77.7	-0.7	27.4	-19.4	29.8
Mid-shelf (44 m) (Mar-July 1978)	1.8	39.2	-36.7	80.8	-1.6	25.1	-14.5	21.9
Inner shelf (10 m) St. Lucie Inlet	-1.1	44.0	-36.2	164.4	-1.6	17.4	-13.3	15.2

Variance of the along-shelf component was about 3 to 4 times greater than the cross-shelf component at the mid-shelf site. On the inner shelf, the along-shelf energy was an order of magnitude greater than cross-shelf energy. Relatively greater energy parallel to the shoreline in the inner shelf data set may result from several factors, including the presence of a tidal inlet, the relatively short record may have coincided with an unusually active time period, and nearshore regions may be more energetic than deeper areas further offshore.

Numerical analyses of these data sets showed energy concentrated at particular spectral bands. Spectral density estimates were derived for these data sets and presented as variance-preserving spectra (Figure 5-4). Largest areas beneath the curves represented the greatest spectral energy content. Most energy was in the along-shelf component in the band 0.1 to 0.5 cycles per day or periods about 2 to 10 days. There were sharp peaks at the diurnal and semi-diurnal bands, representing the principal tides, but these contained little of the overall energy, as tidal peaks were quite thin relative to lower-frequency bands. There was significant cross-shelf energy in the semi-diurnal band from June to November, less semi-diurnal energy from March to July. Subtidal energy in the cross-shelf direction was weak. Most current energy at the mid-shelf location was contained in along-shelf subtidal frequency bands.

5.1.1.2 Current Components

Harmonic analysis of the data sets removed selected tidal constituents from the records, isolating the residual, or non-tidal currents. Calculation of variance for these tidal constituents revealed that tides at the mid-shelf location were weak, accounting for about 5% of the overall current energy. The residual signal dominated mid-shelf observations. Peak tidal speeds at mid-shelf were about 5 cm/sec; tidal ellipses were parallel to the bathymetry but eccentricity was low (more circular). Tides on the inner shelf near St. Lucie Inlet accounted for 30% of the overall current variance. Inner shelf tidal variance was greater in the along-shelf component than the cross-shelf component; scatter plots of tidal currents show ellipses oriented parallel to the shoreline. Peak tidal current speeds near St. Lucie Inlet approached 20 cm/sec.

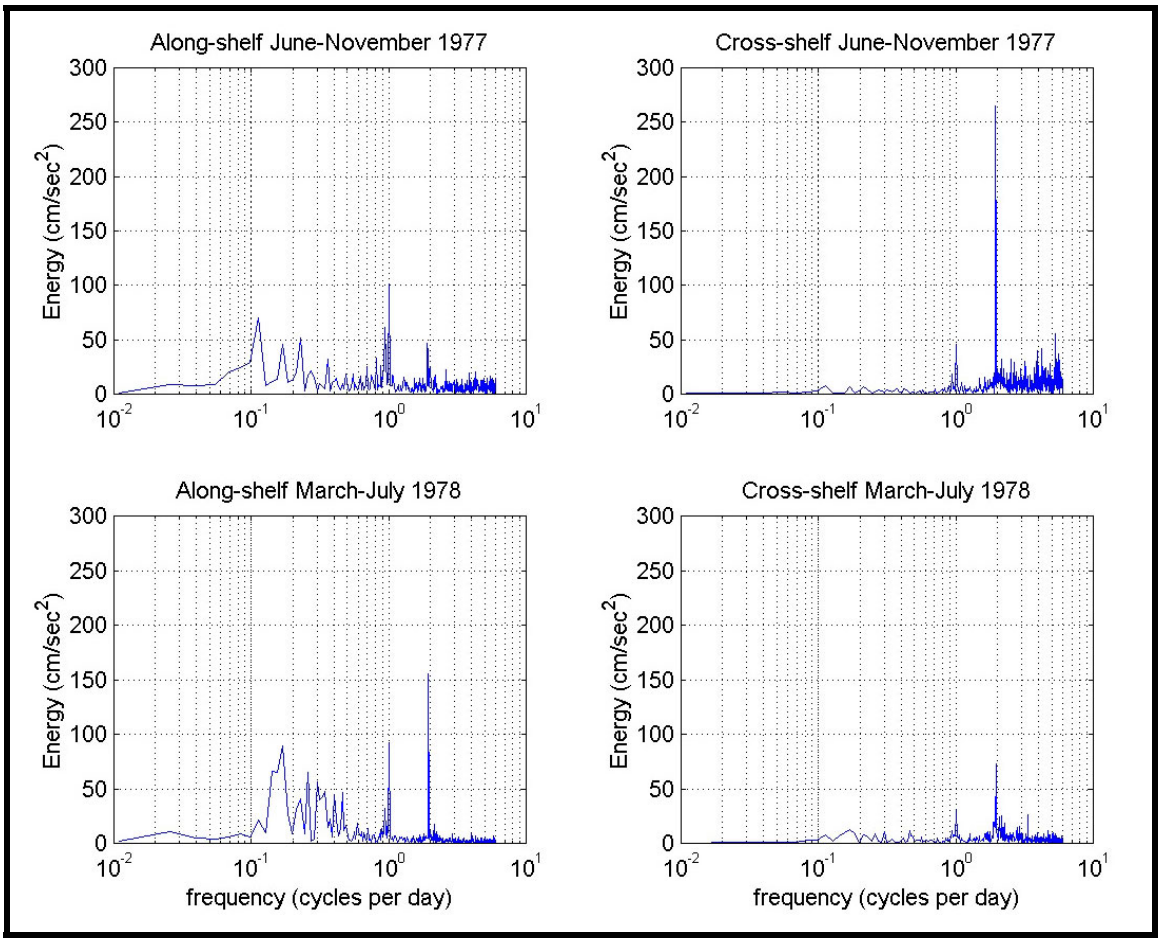

Figure 5-4. Variance-preserving spectra for mid-shelf current meter observations presented in Figure 5-1. Subtidal processes (frequencies less than 1 cycle per day) contained most of the current energy; along-shelf energy was 3 to 4 times greater than cross-shelf energy.

The residual signal represented current motions due to non-tidal processes. These signals were reduced further with a 33-hour low-pass filter to remove high frequency noise. The remaining subtidal signal represented current processes at lower frequencies, currents shown to contain significant spectral energy (Figure 5-4). These currents were found to possess more than half of the total current energy at the inner shelf location and between 60% and 75% of the total energy at the mid-shelf location. Subtidal processes were responsible for the periodic high-speed events observed in the original time series (Figures 5-1 and 5-2).

Two primary forcing influences, winds and Florida Current eddy effects, were investigated as potential causes for subtidal energy. Correlation between wind stress near St. Lucie Inlet and currents at the mid-shelf location accounted for about 10% of the along-shelf subtidal variance predicted by along-shelf wind stress. Correlation improved when along-shelf winds were compared with cross-shelf flow; about 18% of the cross-shelf variance could be predicted by wind stress. Correlations were better for the March to July data set than for the June to November data set. About 1% of the cross-shelf and along-shelf variance was explained by cross-shelf wind stress. The higher correlation

between cross-shelf currents and along-shelf wind stress may be due to Ekman dynamics; a northward wind stress may cause currents in the surface layer to veer slightly to the right of the wind direction or offshore. Bottom currents then would be drawn shoreward (or to the left) to balance the induced pressure deficit (Pickard and Emery, 1990).

On the inner shelf near St. Lucie Inlet, subtidal currents generally moved in the direction of wind stress. About 26% of the along-shelf current variance was predicted by along-shelf winds, and about 10% of the cross-shelf current variance was due to winds.

According to the literature, most current energy on the southeast Florida shelf can be attributed to meanders or spin-off eddies generated from the Florida Current (see Section 2.2). These perturbations of the Florida Current propagate northward along the Florida shelf as wave-like filaments or counter-clockwise rotating eddies. These processes have great influence on the outer shelf where water depths are greater than about 75 m, with their influence diminishing into shallow water on the inner shelf. Eddies have time scales of approximately 2 to 14 days, depending on location and time of year (Lee, 1975; Lee and Mayer, 1977; Lee and Mooers, 1977; Santos, et al., 1990). Spin-off eddies transport subtropical water from the Florida Current onto the shelf (Lee and Mayer, 1977), and also induce onshore upwelling of deeper, cooler water (Zantopp et al., 1987). The result can be sharp temperature gradients surrounding the eddy.

Comparison of subtidal current variability with temperature variability at the mid-depth site yielded mixed results between the two time periods. From June to November 1977, 21% of the cross-shelf current variability and 8% of the along-shelf current variability could be predicted by temperature changes. However, from March to July 1978, these percentages fell to about 2%, suggesting most subtidal variability may be due to indirect response to meanders, spin-off eddies, or other manifestations of the Florida Current.

5.1.2 Field Data Collection

Field measurements of currents over Thomas Shoal and within Areas B1 and B2 were conducted Fall 2000, Spring 2001, and Fall 2001. The purpose of these measurements was to observe spatial and temporal flow variability over a shoal typical of a potential sand resource area in central east Florida. Results of the surveys yielded observations on flow variations in a localized region and were used in concert with long-term historical current data to augment our understanding of flow characteristics on the inner-continental shelf off central east Florida. Observations support the results of historical data analyses, suggesting flow offshore central east Florida was dependent on local variations in wind conditions, regional patterns of the Florida Current, and local bathymetry. Tidal effects seem to be minor in comparison with other forcing mechanisms.

This section briefly describes field data collection procedures, including instrumentation, survey techniques, and data processing. Furthermore, flow conditions observed at the survey site are discussed. Setup conditions determining flow characteristics (i.e., winds and tides) were different during fall and spring surveys. The following describes how flow in Areas B1 and B2 responded to different forcing conditions. All current measurement plots are presented in Appendix D.

5.1.2.1 Survey Instrumentation and Techniques

The surveys were designed to measure currents across a central portion of the study area during an approximate 24- to 48-hour period under fall and spring conditions. A

pre-defined set of transect lines were traversed at regular time intervals intended to span two to four complete tidal cycles to evaluate the spatial and temporal variation in current structure in the study area (Figure 5-5).

The survey transect grid was composed of eight lines designed to approximate a square figure-8 pattern. The survey grid extended approximately 7.6 km in the along-shelf direction and 4 km in the cross-shelf direction (Figure 5-5). The center line of three parallel cross-shelf lines was located perpendicular to the axis of the shallowest region of the sand shoal. The vessel began surveying in the northeast corner of the grid and traveled southeast (along-shelf) to the intersection with the center line (Line 1). The vessel rotated to the west, and traveled southwest across the shoal (cross-shelf, Line 2). Line 3, from the center line to the southwestern corner of the survey grid, was traversed in a southeast direction (along-shelf).

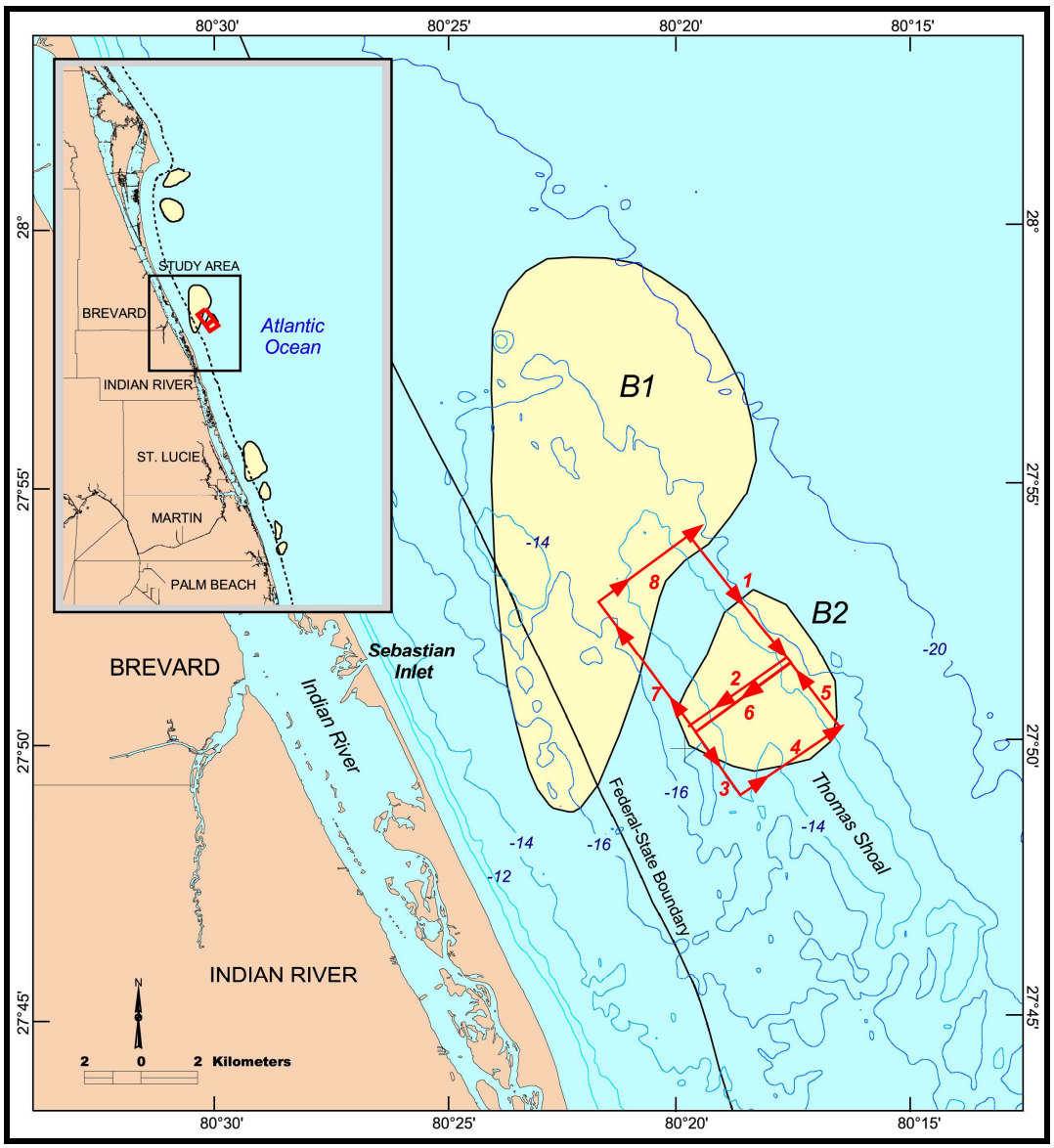

Figure 5-5. Bathymetric map of study area showing the ADCP survey line pattern displayed in red.

With the vessel on a northeast heading, the southern cross-shelf line was traversed to the southeastern corner of the grid (Line 4). Line 5 was run along-shelf, from the southeast corner of the grid to the intersection with the center line, and the center line was traversed a second time from northeast to southwest (Line 6). The vessel rotated to the north and proceeded in a northwest (up-shelf) direction traversing Line 7. Cross-shelf Line 8 closed the pattern, extending from the northwest corner of the grid to the northeast corner. Each line was completed in approximately 30 minutes, with an entire eight-line cycle traversed every 4 hours, surveying the centerline every 2 hours. This survey technique provided adequate spatial coverage of Areas B1 and B2, and it was designed with the cross-shelf bias to observe along-shelf flow, the more dominant process.

Each proposed survey would allow the completion of 12 cycles in a 48-hour period. Two cycles were completed during the Fall 2000 survey, and six cycles were completed during Spring and Fall 2001 surveys. The initial survey, September 19, 2000, was conducted aboard a 41-foot charter fishing boat, *Luna Sea*. The survey began at 0915 on September 19, but instrumentation problems delayed current measurement collection until 1645 hours. Although weather conditions in the morning on September 19 were favorable for surveying, wind speeds slowly increased throughout the day. At 1700 hours, wind gusts up to 7 m/sec were reported at the National Data Buoy Center (NDBC) station offshore Cape Canaveral. Winds blew out of the southeast causing large swell to propagate northwest along the axis of the survey grid. By 0500 on September 20, wind speeds reached 11 m/sec with gust up to 13 m/sec. The survey was terminated at 0322, September 20, when high speed, southeasterly directed winds made navigation of cross-shelf transect lines impossible. The September 2000 survey results showed pitch and roll of the boat was more variable than the instrumentation could resolve, resulting in a lack of confidence in current data measured under the given weather conditions.

The May 2001 survey was conducted aboard a 32-foot charter fishing vessel, *My Last Fling*. The survey began at 1947, May 29, and six cycles were completed before the survey was terminated at 2200 on May 30 due to unfavorable weather conditions. Details of this survey are discussed in Section 5.1.2.2. The fall survey was repeated in September 2001. Based on our experience and May 2001 survey results, a 24-hour current measurement survey was planned. At 1900 on September 4, 2001, the survey commenced aboard the Research Vessel *Barb-N-T*. Six survey cycles were traversed, concluding at 2000 on September 5; results are discussed in Section 5.1.2.3.

Currents were measured using an acoustic doppler current profiler (ADCP) mounted rigidly to a small vessel. The ADCP provided high-resolution measurements of the vertical structure of current flow beneath the instrument transducer. When mounted to a moving platform, such as a small vessel, and used to traverse regional areas, the result is a detailed synoptic view of the current field.

The ADCP was configured to balance maximum accuracy with reasonable vertical resolution, resulting in a standard deviation (or accuracy of current measurement) of approximately 1.3 cm/sec. Vertical resolution was 0.5 m or one velocity observation every 0.5 m water depth. Each vertical profile took approximately 4 sec to collect. Averaging parameters resulted in a horizontal resolution of approximately 10 to 12 m along a transect line.

Position information was collected using HYPACK®, an integrated navigation software package running on a personal computer, linked to a Trimble Pro XR differential GPS.

Position data were recorded in Universal Transverse Mercator (UTM) NAD83 coordinate system in meters. Position updates were available every 2 sec, although brief interruptions of position data were experienced when thunderstorms were in the area. These brief losses of position data (less than 10 sec) did not compromise results.

Surveys resulted in two types of data: current velocity profiles (or ensembles) and vessel position. ADCP data for a single transect consisted of velocity components at every depth bin for each profile. For these surveys, the two earth-referenced velocity components (V_{east} and V_{north}) were reported, as well as current speed, current direction, and error velocity. The conversion process outputs each ensemble profile as a function of depth (i.e., V_{east} versus depth, V_{north} versus depth, etc.). A series of ensemble profiles along transect line were recorded in each data file.

Time-stamped position data as northing and easting were recorded within HYPACK®. The ensemble profiles were merged with the position data to assign a unique x-y pair to every ensemble. This merging operation was done using time as the common link between HYPACK® and ADCP data files. By searching for the unique position at a specific time for each velocity profile, an accurate x-y location was assigned to each ensemble.

Current measurements are presented as vector maps throughout the survey areas. The vector maps represent vertically-averaged current velocities at specific locations within the survey domain. Velocity profiles were separated into near-surface, mid-depth, and near-bottom layers, with an average velocity value calculated for each depth layer. Vectors corresponding to a single survey cycle (8 transect lines) then were displayed on an area map. These vector maps were produced for the surface, mid-depth, and bottom layers for each of the six survey cycles. A series of plots shows temporal and spatial variation in horizontal and vertical currents during the survey. A complete set of vector maps for each survey is presented in Appendix D.

5.1.2.2 Spring 2001 Survey Results

Areas B1 and B2 were surveyed May 29 and 30, 2001. Thomas Shoal has a bathymetric relief of about 5 m that influences local circulation patterns approximately 5 km east of Sebastian Inlet (Figure 5-5). The shoal is crescent shaped with the major axis oriented northwest-southeast, approximately parallel to the orientation of the shoreline. The southern portion of the shoal extends towards shore, creating an onshore concavity.

Wind speed and direction were obtained for the survey period from an NDBC buoy 20 nm east of Cape Canaveral. In the days preceding the survey, winds were generally blowing from the south at 5 to 10 m/sec (Figure 5-6). Winds shifted north-northeast 5 days before the survey.

These northerly winds reached a maximum of 8 m/sec and then abated. On May 26, winds rotated south in a clockwise direction, reaching a maximum of almost 12 m/sec. On May 29 and 30, strongest winds blew out of the south-southwest, starting at 4 m/sec and increasing to as much as 8 m/sec. From 0100 to 1200 hours on May 30, winds shifted to the west-northwest decreasing in speed from 4 to 1 m/sec. Afternoon winds were southeast to east, reaching speeds of 6 m/sec. Field notes taken during the survey document increasing winds and waves leading up to a storm that passed through the area terminating the survey in the evening of May 30.

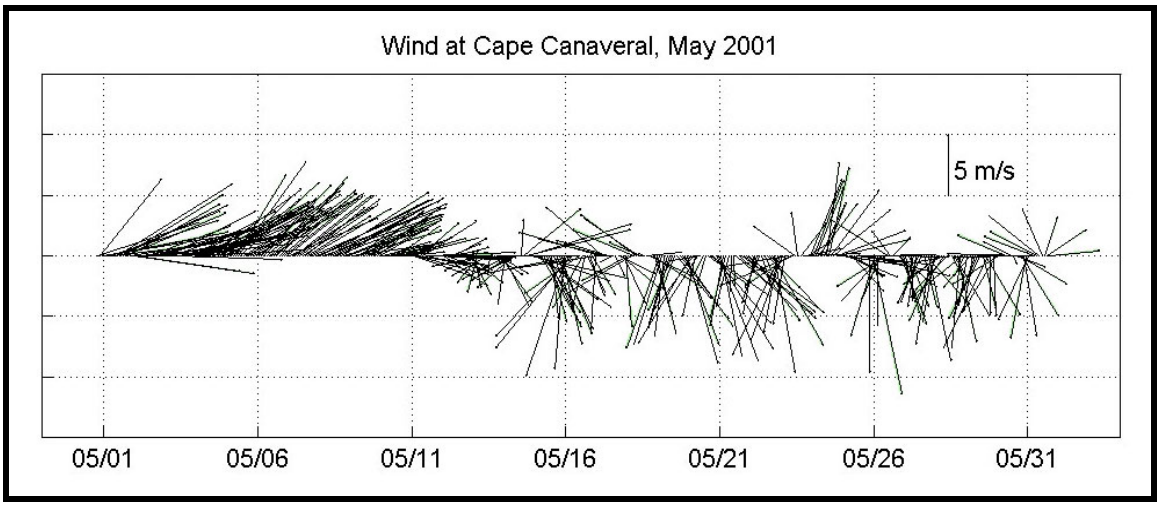

Figure 5-6. Wind conditions prior to and during the May ADCP survey measured at the NDBC buoy 20 nm east of Cape Canaveral.

Tidal elevations during the survey were collected from a NOS tide gage at the Trident Pier in Port Canaveral. Semi-diurnal tides dominate the region, specifically the M2 and S2 tidal constituents, resulting in two highs and two lows each day (Figure 5-7). On May 29, the survey began at 2035, coincident with the second low tide of the day. The survey ended on May 30 at approximately 2200 hours, 2 hours after the evening low tide, spanning two complete tidal cycles. The maximum tide range was 1.1 m.

Currents during the May survey were dominated by an underlying mean northward flow that was modified on the surface by winds and steered by bathymetry near-bottom (Figure 5-8). On the perimeter of the shoal, surface current speeds of 10 to 25 cm/sec correlated well with wind direction; winds out of the southwest drive a northerly flow. Across the shallowest portion of the shoal, surface flow was deflected onshore by local bathymetry. Near-bottom currents with speeds of 5 to 20 cm/sec typically flow up-shelf parallel to bathymetric contours. Cycle 1 current measurements suggest Ekman transport; surface currents veer right of wind direction (offshore), and bottom currents are drawn shoreward in response to a northward wind stress (Pickard and Emery, 1990). Ekman transport off the southeast coast of Florida is explained more thoroughly in Section 2.2. The circulation pattern described is illustrated in Figure 5-8 by the northeast surface current and the northwest bottom along Line 1. Ekman transport creates potential for upwelling, which persists into Cycle 2 but with less force due to a shift in wind direction.

Horizontal variability of currents measured mid-way through the May survey (Cycles 3 and 4) are not thoroughly explained by direct wind-forcing. As the wind shifted west-northwest, surface currents on the eastern side of the shoal flowed strongly to the east, while the mean underlying northward flow of bottom currents was impeded (Figure 5-9). On the western side and across the center of the shoal, surface and near-bottom current speeds were reduced. As wind speeds decreased (Cycle 4), surface currents slowed, but northerly-flowing near-bottom currents increased in energy (Figure 5-10). This underlying northerly mean flow, most clearly observed in near-bottom currents, was likely an indirect effect of the Florida Current. As discussed in Section 2.2, the frontal zone of the Florida Current meanders along the shelf break (approximately 40-m isobath). However, spin-off eddies along the western edge of the Florida Current have induced flow along the middle

(20- to 40-m isobaths) and inner shelf (shore to 20-m isobath). In winter and spring months, eddies propagate northward in response to southerly winds (Lee and Mayer, 1977). Florida Current eddies typically scale 10 km in the cross-shelf and 20 to 30 km along the shelf, forming every 2 days to 2 weeks, and historically have accounted for current variability that is poorly correlated with wind stress. During survey Cycles 4 and 5, decreasing speeds of surface currents correlated with decreasing wind speeds, but increased speeds of northerly bottom currents could not be explained by wind or tidal conditions. However, attributing these effects to the Florida Current is a bit speculative because the spatial and temporal scales of this survey are not adequate to resolve Florida Current effects.

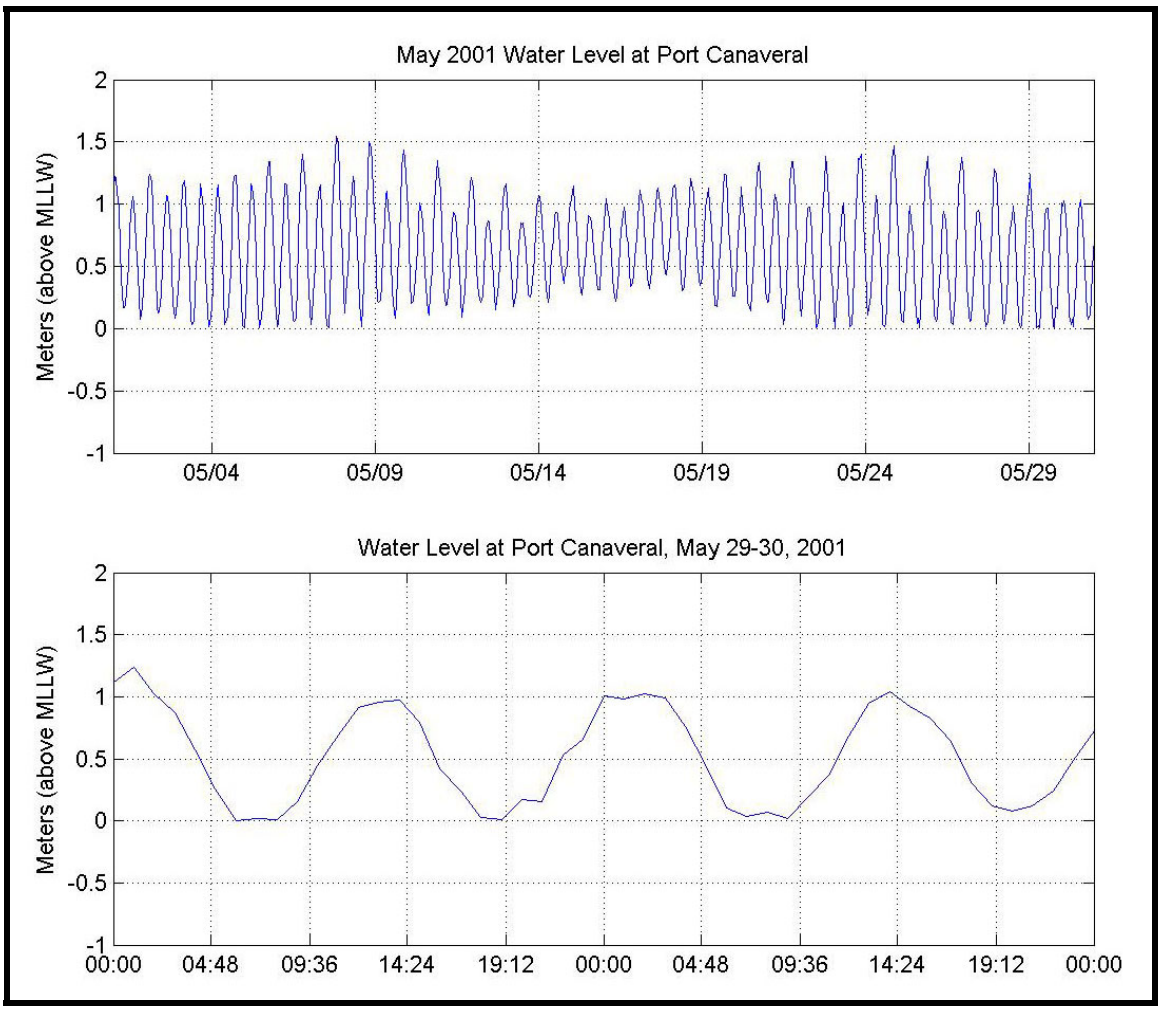

Figure 5-7. May 2001 water elevation measured at the NOS tide gage on the Trident Pier at Port Canaveral; the lower plot illustrates water level during the survey.

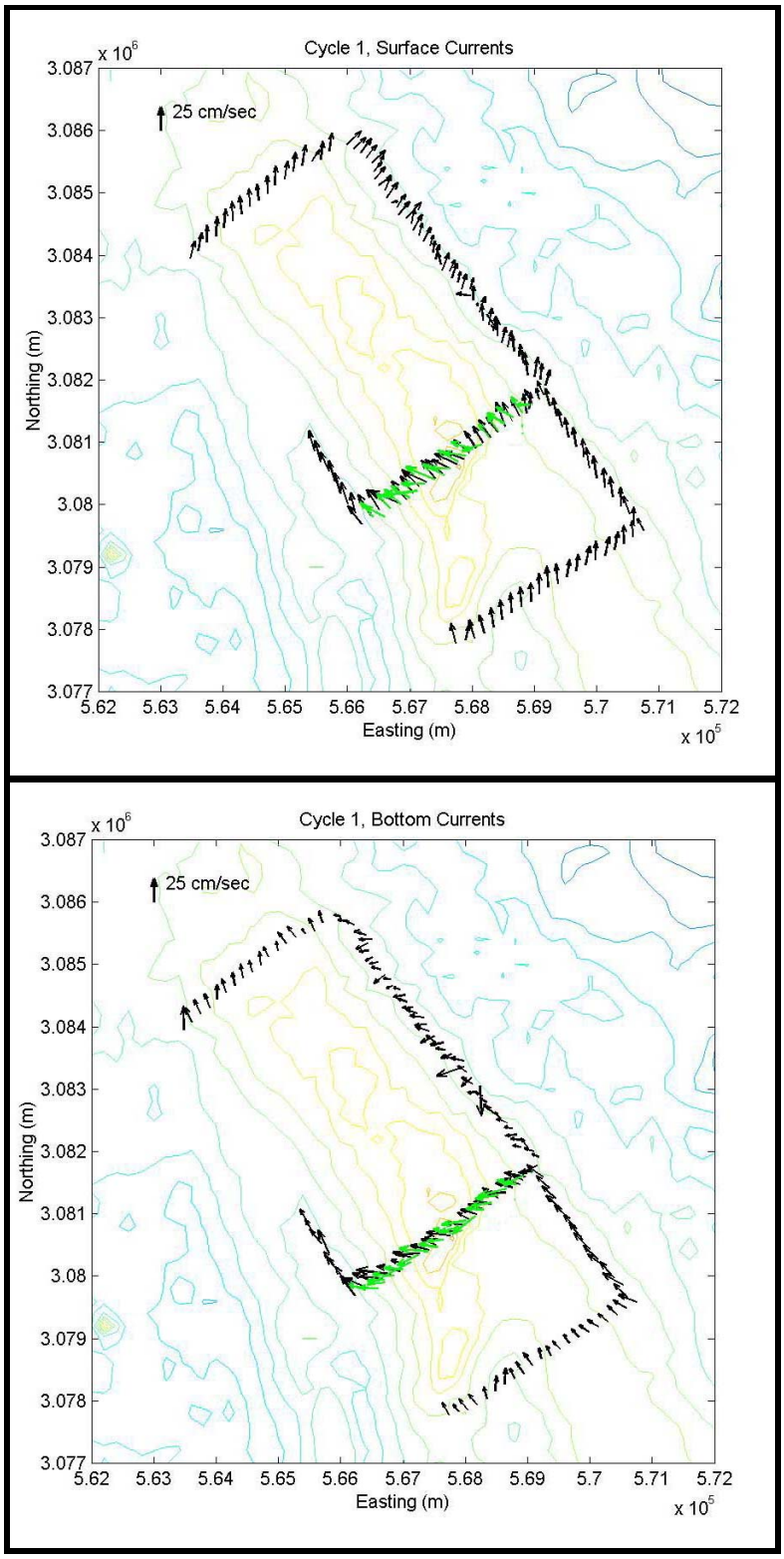

Figure 5-8. Cycle 1 (May 29, 2001 survey) current measurements illustrate a mean northward flow, with an onshore component across the shallowest portion of the shoal.

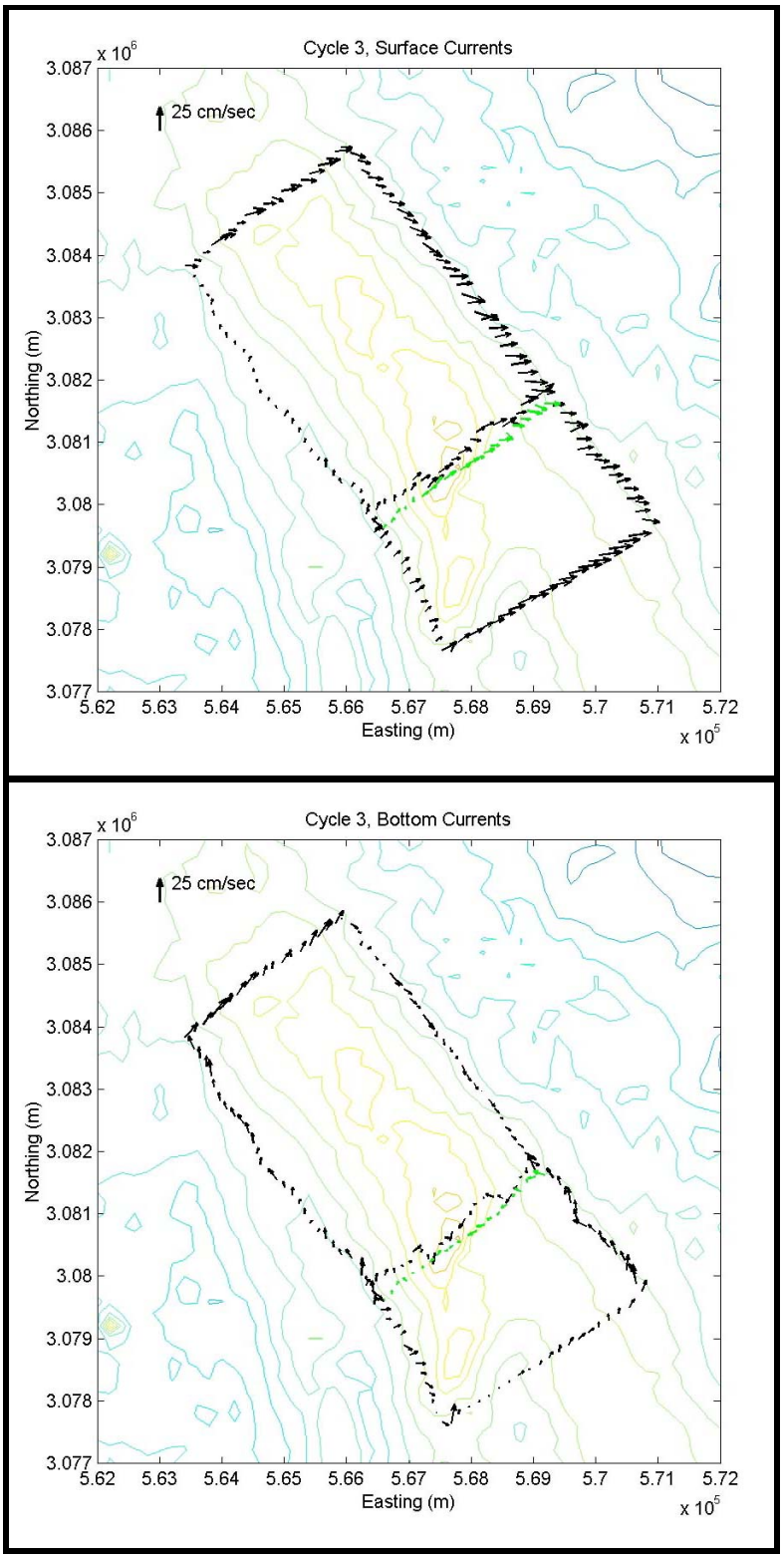

Figure 5-9. During May survey Cycle 3, surface currents on the eastern side of the shoal flowed strongly to the east, while the mean underlying northward flow of bottom currents was impeded. On the western side and across the center of the shoal, surface and near-bottom current magnitudes were reduced significantly.

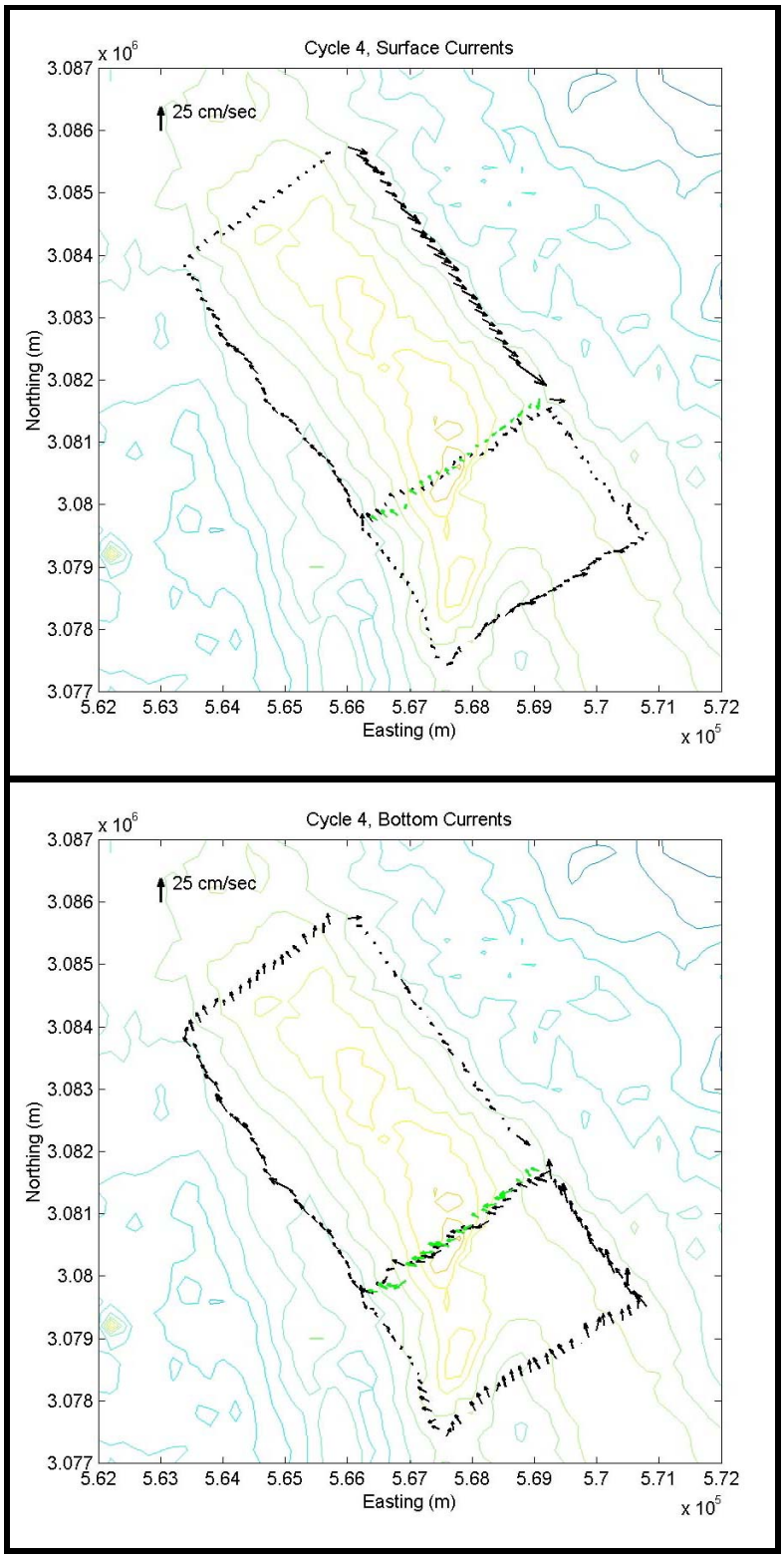

Figure 5-10. During May survey Cycle 4, surface currents slowed due to decreasing winds, but northerly flowing near-bottom currents increased in energy, possibly an indirect result of the Florida Current.

Although current speeds throughout the water column increased with increasing wind speed into Cycle 6, the spatial variability of currents was erratic. Increased wave action, documented in field notes, was likely the cause of extreme current magnitudes and inconsistent flow direction near the end of the survey. Wave-induced flow could not be resolved accurately using ADCP shipboard measurements. A combination of large errors in ADCP measurements and thunder and lightning storms terminated the May 2001 survey.

The water column was weakly stratified at the beginning of the spring survey. Wind-generated storm events and decreased surface water temperatures during winter months commonly results in some mixing. Near-bottom current speeds tended to be slightly slower than surface currents for any given time during the spring survey. Along the perimeter of the shoal, most energy was contained in the along-shelf current component, but across the shoal, cross-shelf currents dominate. Across the shallowest portion of Thomas Shoal, transect Lines 2 and 6 (Figure 5-5), currents seemed to be tidally influenced. Cross-shelf currents flow strongly onshore with speeds up to 25 cm/sec during flood tide (Cycle 1, Figure 5-8). On the ebb tide, cross-shelf currents at speeds of less than 10 cm/sec were directed offshore (Cycle 3, Figure 5-9). These results suggest that onshore cross-shelf currents were favored and enhanced during flood tide cycles. Tidal-induced flows at the southern and northern cross-shelf transect lines were insignificant.

5.1.2.3 Fall 2001 Survey Results

Currents in the vicinity of Thomas Shoal were measured for the fall season on September 4 and 5, 2001. Spring survey transects were repeated to determine the characteristics of seasonal flow variability from spring to fall. Wind speed and direction from the NDBC buoy off Cape Canaveral indicated winds blowing from the south at 5 to 7 m/sec (10 to 14 kts) during the weeks preceding the survey (Figure 5-11). However, winds shifted and blew from the north between August 25 and 30 (5 days before the survey). These northerly winds reached a maximum of 10 m/sec. On September 4 and 5, the wind record showed counterclockwise rotating winds. At the beginning of the survey, strong winds blew from the east-southeast and gradually lost energy as they rotated to the north in the first 12 hours. Wind speeds were below 3 m/sec from 0000 to 1400 hours on September 5. As winds shifted to a more southerly direction at 1500 hours, wind speeds exceeded 4 m/sec throughout the remainder of the survey.

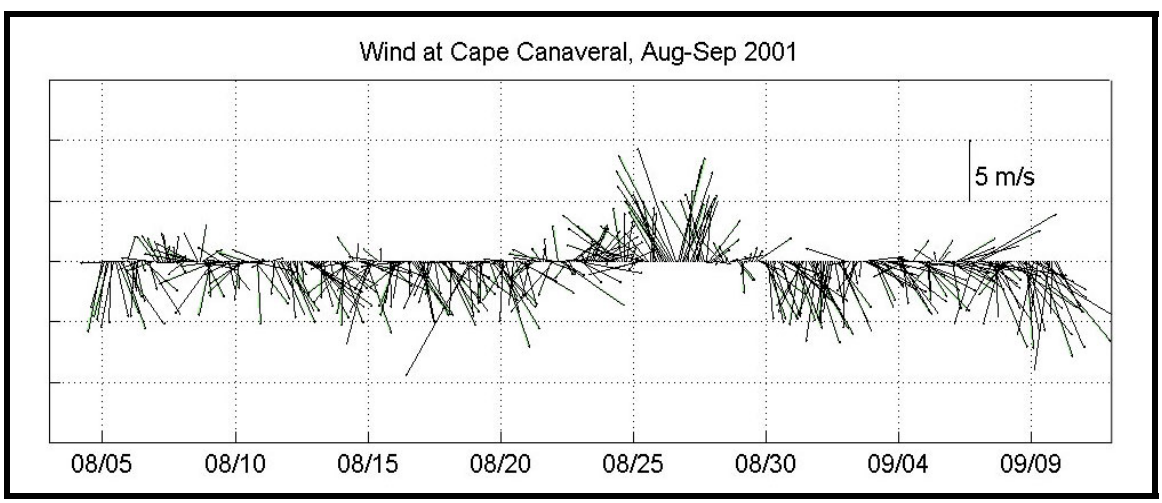

Figure 5-11. Wind conditions prior to and during the September survey measured at the NDBC buoy 20 nm east of Cape Canaveral.

On September 4, the survey began at 1900 hours, just prior to the second high tide of the day. The survey ended on September 5 at approximately 2000 hours, 1 hour prior to the latter high tide, spanning almost two tidal cycles. Maximum tide range on this day was approximately 1.0 m at Cape Canaveral (Figure 5-12). Based on annual tide records, September 4 and 5 correspond to nearly spring tides (maximum tidal range). However, the tidal record shows the 14-day spring tide cycle from August 27 to September 10 has a lower than average maximum range of 1.1 m (Figure 5-12). This reduced tide range may have been due to the period of strong northerly winds in late August.

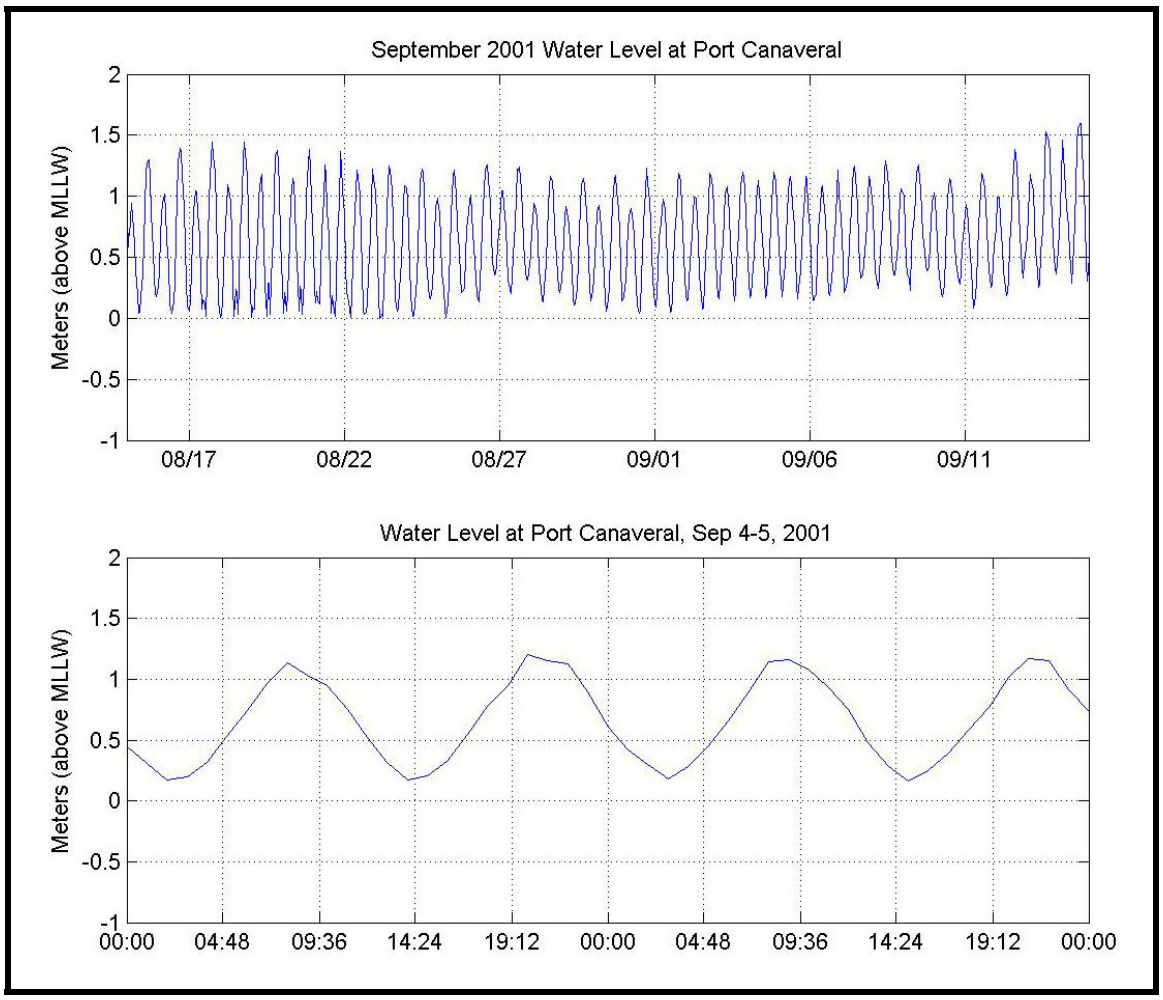

Figure 5-12. September 2001 water elevation measured at the NOS tide gage on the Trident Pier at Port Canaveral; the lower plot illustrates water level during the survey.

September survey results illustrated a mean southerly flow that was altered by wind direction. Leading up to Cycle 1, winds had been blowing out of the east-southeast for several hours. Surface currents on the eastern side and across the center of Thomas Shoal flowed to the west and southwest at approximately 20 cm/sec in response to easterly winds (Figure 5-13). Bottom currents flowed southeast aligned with bathymetry. Opposing surface and bottom current directions suggest Ekman dynamics in the presence of southeast winds. However, rotating winds beginning in Cycle 2 obscure the subtle indication of Ekman circulation. Across the shoal, currents throughout the water column were dominated by onshore cross-shelf flow.

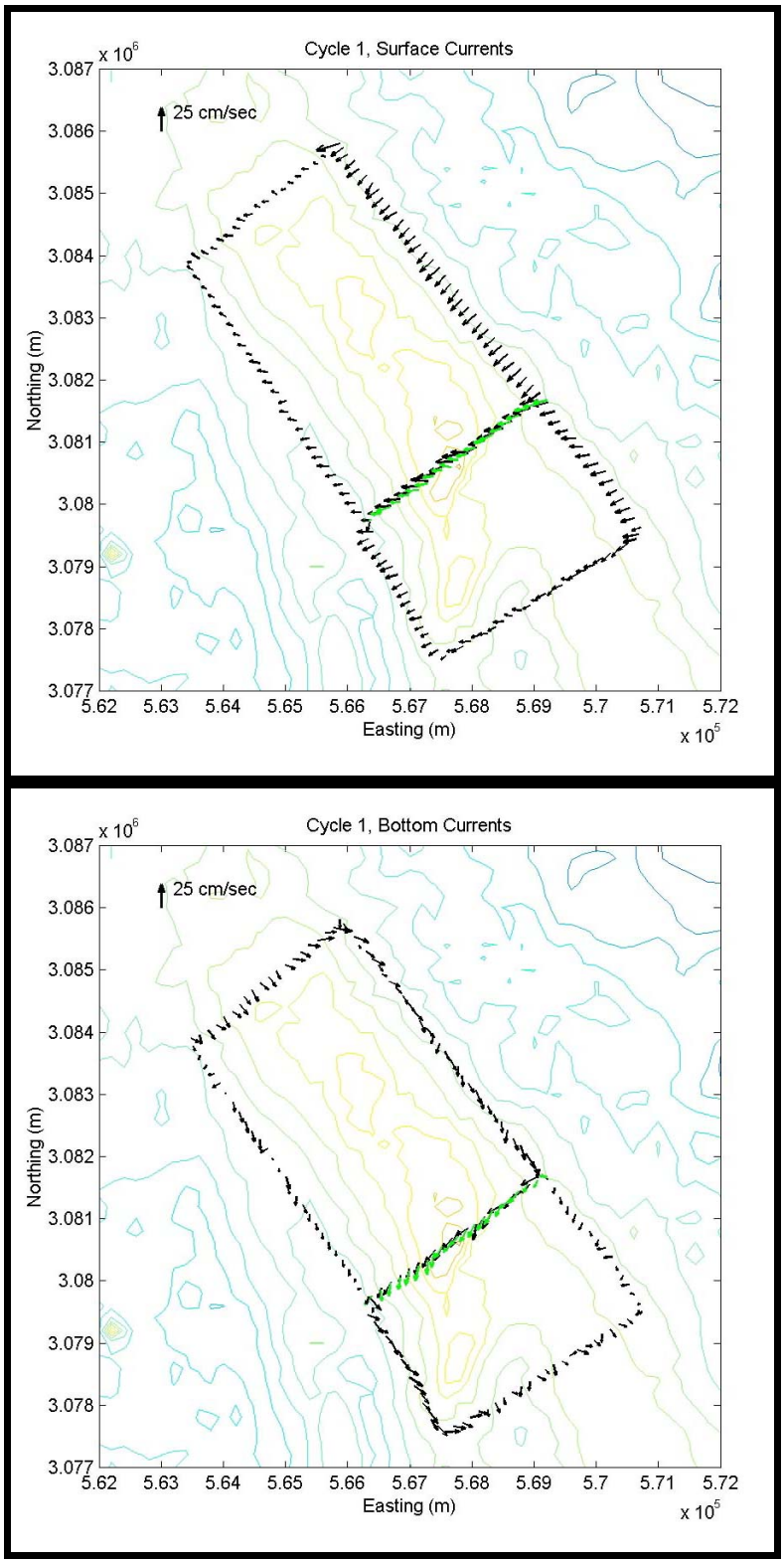

Figure 5-13. During September survey Cycle 1, surface currents on the eastern side and across the center of the shoal flowed to the southwest due to easterly winds. Bottom currents flow southeast, aligned with bathymetry.

Current speeds were strongest (20 to 30 cm/sec) in the presence of northerly winds. During survey Cycles 4 and 5, winds rotated counterclockwise sustaining an average speed of 2 m/sec. Winds blew from the west at the beginning of Cycle 4 (0800, September 5), rotating north in the middle of Cycle 4 (1000 hours), northeast at the beginning of Cycle 5 (1200), and east by the end of Cycle 5 (1500). In response to northerly wind, surface currents gradually increased in speed during Cycle 4 and shifted in direction from south to southeast along bathymetric contours (Figure 5-14). Maximum surface current speeds of 30 cm/sec flowing to the southeast were reached during Cycle 5 (Figure 5-15). Maximum bottom current speeds of 25 cm/sec also were observed during the short period of northerly winds (Figure 5-15). Bottom currents maintained a southerly direction aligned with bathymetric contours throughout the survey, and were enhanced by northerly winds. The response of bottom currents to wind shift was delayed compared with surface currents. During Cycle 4, bottom current speeds were less than 15 cm/sec (Figure 5-14). Bottom current speeds along the eastern side and across the shoal increased in energy during Cycle 5, but remained weak along the western margin of the shoal (Figure 5-15).

Along the perimeter of Thomas Shoal, there was an indication that bottom currents vary with proximity to the shoal. Measurements along Line 7, on the western margin of the shoal, showed an average water depth of 15 m; the shallowest depth across the shoal was approximately 11 m. Flow along Line 7 was weaker than on the eastern margin of the shoal (14 m water depth), and it was directed onshore (Figure 5-15). Weaker bottom currents along the western boundary of the shoal may have resulted from modification of stronger currents as they crossed the shoal (i.e., bathymetric sheltering). In addition, the literature illustrates that wind influence on bottom currents decreases with increasing depth, which may explain the presence of weaker currents along the western margin of the shoal.

Along the shoal perimeter, most of the current energy was contained in the along-shelf component of flow. Figure 5-16 shows vertical profiles of the along-shelf component of flow for survey Line 7, at the western side of the shoal under three wind conditions, to further illustrate wind dependence on currents during the September survey. In the top panel, winds were out of the south, currents were weak, and the water column was relatively homogeneous. Winds out of the east (middle panel) drive stronger along-shelf currents in the upper half of the water column, but bottom currents remain weak. As discussed previously, the strongest surface currents corresponded to northerly winds (lower panel), but bottom currents along this transect remained weak on the leeward side of the shoal, indicating bathymetric sheltering.

At shallow water depths (11 to 14 m) in close proximity to the shoal, the water column was weakly stratified in the presence of southerly or easterly winds. Northerly winds provide mixing, yielding a more homogeneous water column over the shoal. Near-bottom current speeds were slower than surface currents on all transect lines during most cycles of the September survey. Tidal-induced currents had minimal influence on flows in the survey area.

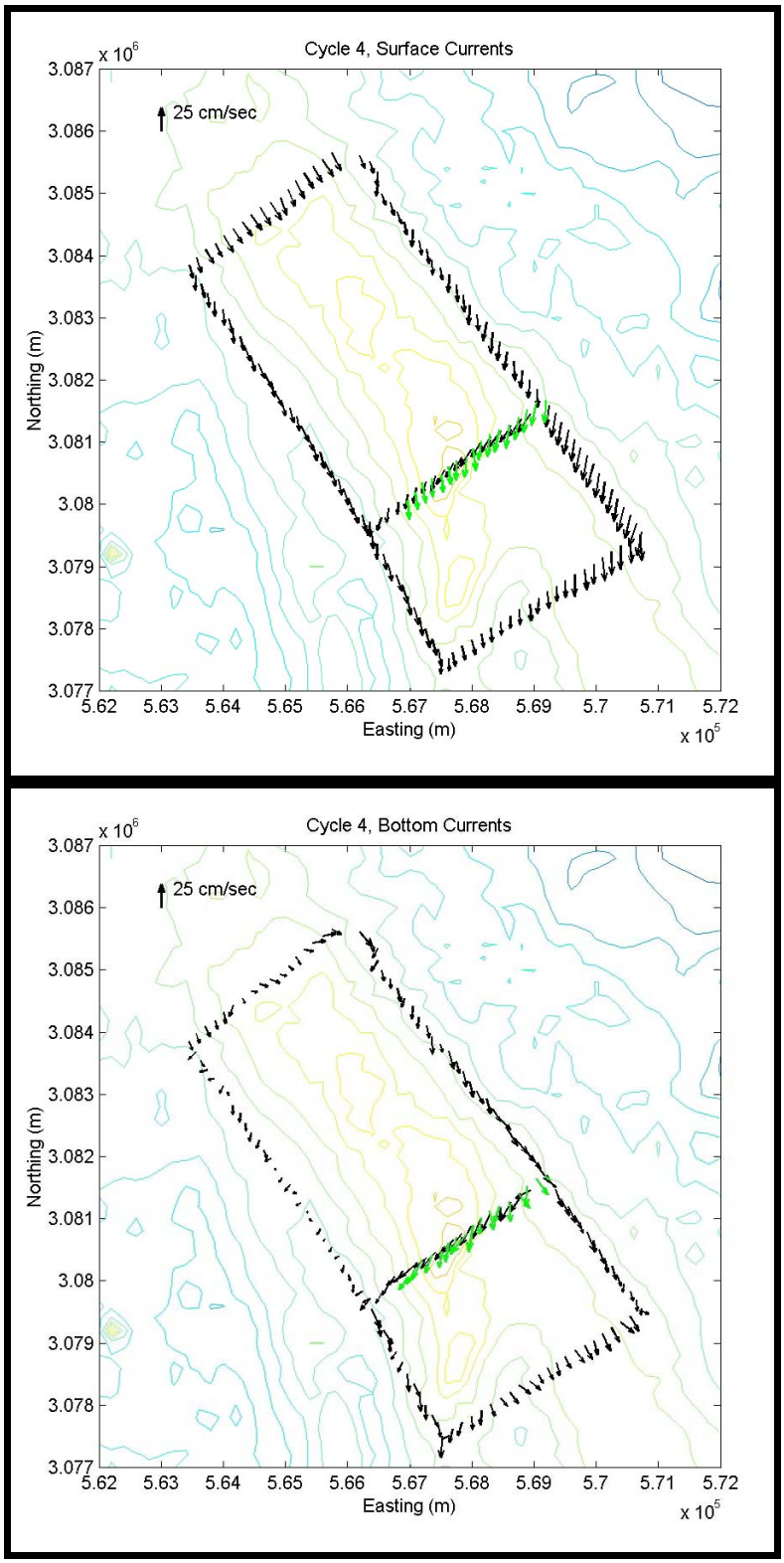

Figure 5-14. In response to the northerly wind, surface currents gradually increase in speed and shift in direction from south to southeast during September survey Cycle 4. Bottom currents do not exhibit a response to this wind shift.

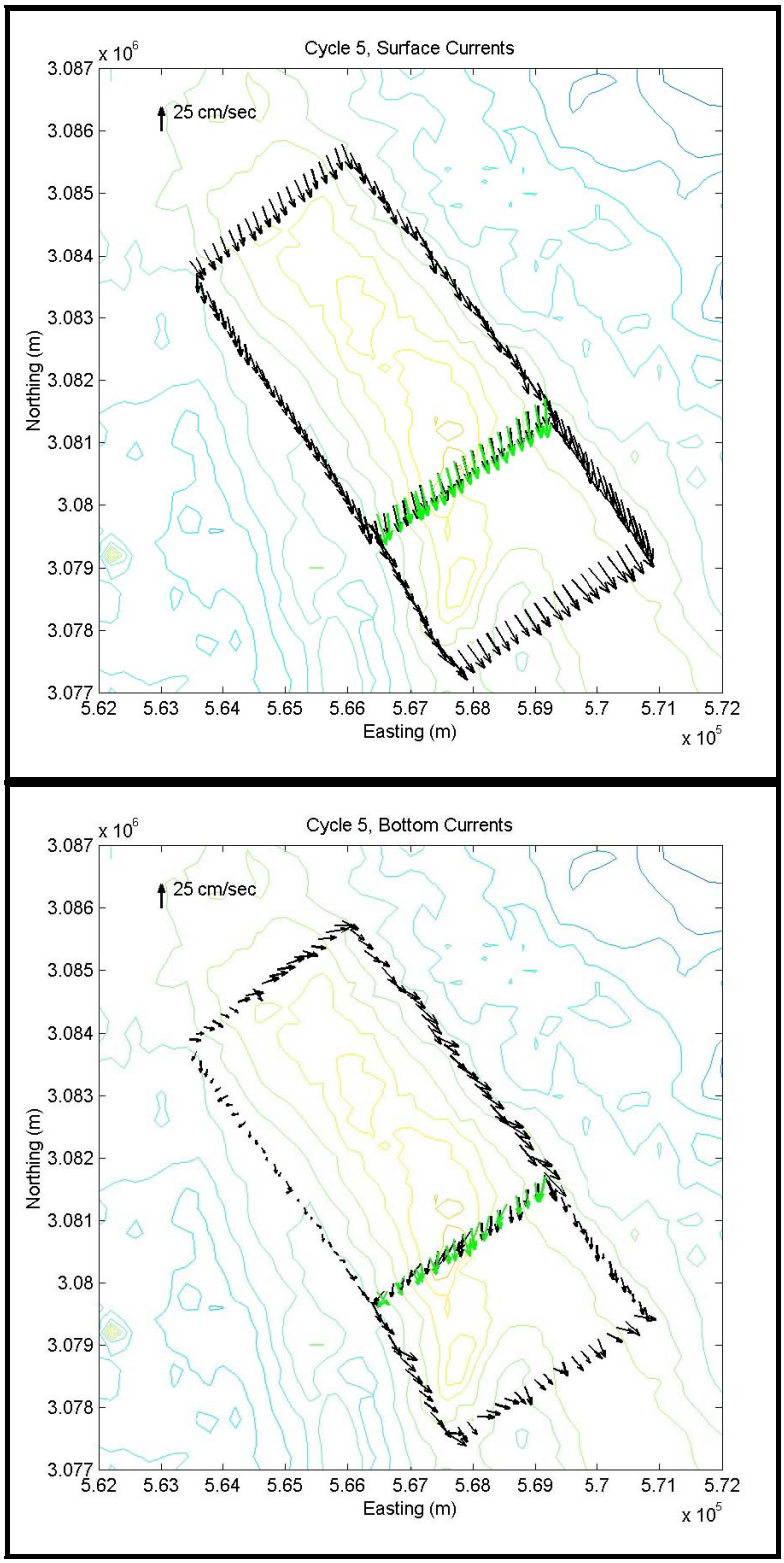

Figure 5-15. Maximum surface current speeds of 30 cm/sec were observed to the southwest and maximum bottom current speeds of 25 cm/sec were reached during September survey Cycle 5 in response to northerly winds.

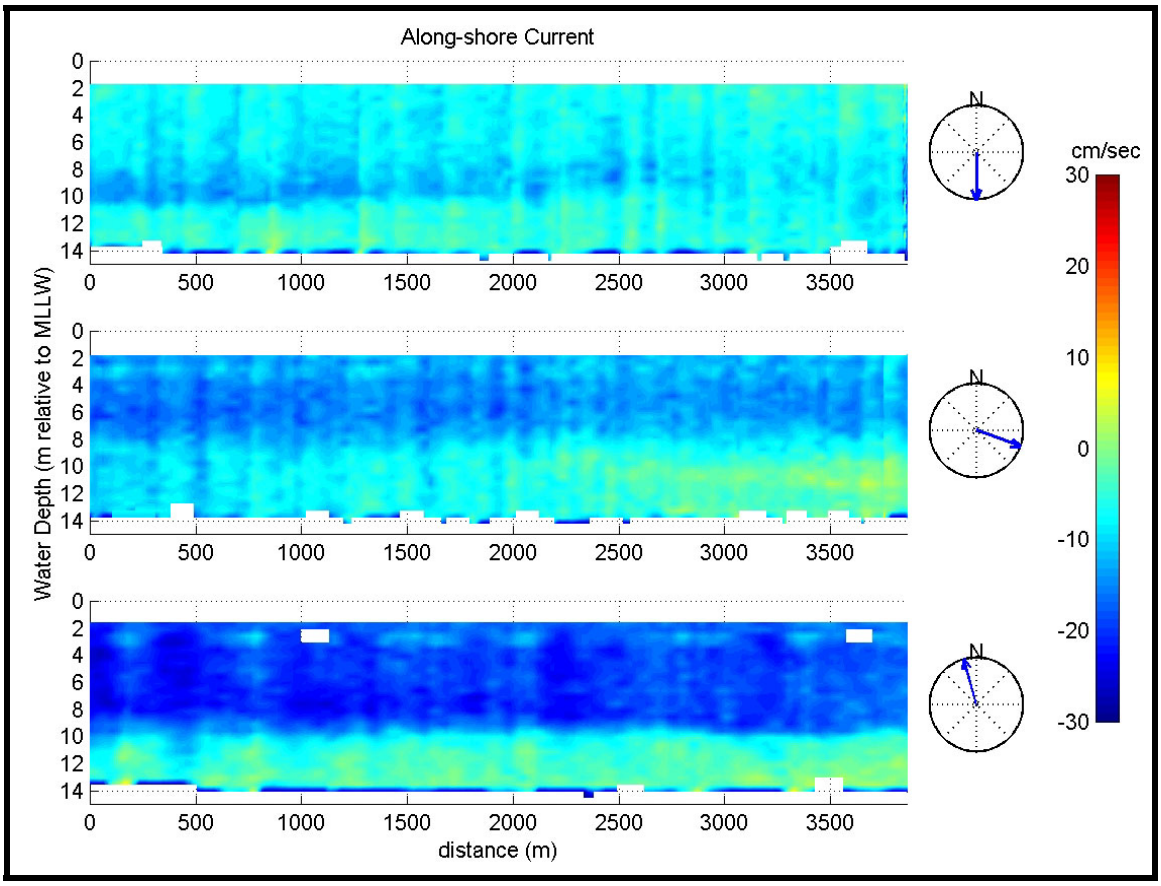

Figure 5-16. Vertical profiles of along-shelf currents measured across Survey Line 7 during three wind conditions indicated by the compass to the right. Positive values (warm colors) indicate currents flowing to the northwest, and negative values (cool colors) indicate currents flowing to the southeast.

5.1.3 Summary of Flow Regimes at Offshore Borrow Sites

Historical current observations and ADCP field surveys indicated that flow regimes in central east Florida were dependent on wind forcing, effects of the Florida Current, and seafloor topography. Tidal currents have minimal influence on flows at borrow site locations.

Circulation patterns along the central east Florida coast near potential offshore borrow sites were investigated using current meter observations obtained offshore St. Lucie Inlet and over Thomas Shoal, seaward of Sebastian Inlet. Analysis of historical data indicated that circulation patterns consisted predominantly of along-shelf currents that reversed direction approximately every 2 to 10 days. Current reversals were found weakly correlated with local wind stress; literature suggested that subtidal variability was due to meanders or spin-off eddies for the Florida Current. Peak speeds were on the order of 40 to 50 cm/sec at mid-shelf and inner-shelf locations and were directed either upshelf (to the north-northwest) or downshelf (to the south-southeast). Strongest currents were most commonly directed to the north. Tidal currents contributed significantly to inner-shelf current observations; however, these observations were obtained near the tidally-dominated St. Lucie Inlet and may not be reflective of inner shelf regions removed from major coastal inlets. ADCP measurements in the vicinity of Thomas Shoal offshore Sebastian Inlet also were dominated

by along-shelf flows that correlated with seasonal changes in wind. May survey conditions were dominated by winds from the south, while September survey conditions were characterized by short wind events from the north. Current measurements illustrated a mean flow directed to the north during spring and to the south in fall. This seasonal directionality of flow was supported by historical data and literature regarding observations on the mid-shelf and inner-shelf where sand resource areas have been identified. Strongest currents flowed to the south at 30 cm/sec during the September survey in response to northerly winds.

Seasonal wind variations have been shown to induce downwelling in winter and upwelling in summer for central east Florida. There was an indication of Ekman transport at the beginning of the May and September surveys. However, wind stress variability during both surveys obscured the subtle indications of Ekman circulation. Based on existing studies, northeast winds in winter will create onshore Ekman transport, inducing downwelling; southeast winds, commonly in summer, drive offshore Ekman circulation, creating potential for upwelling (Smith, 1987).

Current variability not well explained by wind stress may be an indirect response to the Florida Current. The Florida Current flows northward past the study area on the outer shelf (Lee et al., 1985). Instabilities in the Florida Current create spin-off eddies that have been documented on the inner shelf (Smith, 1981). Potential influences of the Florida Current were observed in spring survey results, illustrated by a strong northward flowing bottom current in the presence of weak winds and surface currents. Florida Current effects may enhance northerly flows during winter and spring in the study area.

Tidal effects within the study area are not well documented. In shallow waters, over shoals, and adjacent to tide-dominated inlets such as St. Lucie, cross-shelf tides may influence current velocities. May and September field data showed onshore currents dominated across the shoal. During the May survey, onshore currents were enhanced by flood tide. Tidal dependence was not observed during the September survey. On the inner- to mid-shelf, in the vicinity of the sand resource areas, tidal effects are secondary to wind effects.

In the presence of local bathymetric features, such as Thomas Shoal, steering and sheltering of flow across the shoal were observed. Under average conditions, currents were steered onshore across the shoal. In the presence of dominant winds, near-bottom currents flowed parallel to bathymetric contours. Wind-driven currents across local bathymetric features may not be observed on the leeward side of the shoal. For example, during the May survey, east winds drive southwest currents on the eastern margin of Thomas Shoal, but southeast currents were not observed on the western margin.

5.2 OFFSHORE SEDIMENT TRANSPORT

Infilling rates for potential offshore borrow sites were computed based on a method outlined in Madsen (1987), which relies on earlier work described by Grant and Madsen (1986) for wave-current interaction in the bottom boundary layer outside the surf zone.

On the continental shelf, currents are driven by a combination of forces resulting from winds, tides, and atmospheric pressure gradients. Surface waves also create currents on the sea bottom. These wave-induced currents are oscillatory and fluctuate with the passing of each wave. In Grant and Madsen (1986), the interaction of wave-induced currents

(high-frequency) and background currents with longer time scales (low frequency) was modeled. This analysis provided a method for estimating the combined wave-current friction factor (f_{cw}), which is necessary for computing sediment transport at a borrow site.

5.2.1 Determining Bottom Transport and Infilling Rates

As outlined in Madsen (1987), the net transport q_{net} at the sea bottom in the presence of waves is computed as the averaged instantaneous transport $q(t)$ over the cycle of a wave period T,

$$q_{net} = \frac{1}{T}\int_0^T q_s(t)dt \tag{5.1}$$

The instantaneous value of sediment transport is computed using a formula given by Madsen (1987), which is based on an earlier empirical relationship known as the Einstein-Brown formula (Brown, 1950) for bottom sediment transport in steady unidirectional flow. The Einstein-Brown relationship gives the dimensionless transport rate ϕ as a function of the Shields parameter Ψ,

$$\phi = 40\Psi^3 \tag{5.2}$$

The Shields parameter is used as an indicator of incipient sediment motion, and is the ratio of the shear force τ acting on bottom sediment to the submerged weight of grains. The Shields parameter is expressed as

$$\Psi = \frac{\tau}{(s-1)\rho g d} \tag{5.3}$$

where s is the sediment specific gravity, ρ is the density of water, g is the acceleration of gravity, and d is the sediment grain diameter. The shear stress is a function of the bottom friction factor, f, and the magnitude of the fluid velocity U at the sediment bed. It is expressed as

$$\tau = \frac{1}{2} f \rho U^2 \tag{5.4}$$

A critical value for the Shields parameter is determined using the Shields diagram, which defines the point of incipient sediment motion based on the boundary Reynolds number. For instantaneous values of the Shields parameter that are less than the critical value, no sediment motion will occur.

Therefore, during portions of the wave period that sediment motion does occur, the instantaneous dimensional sediment transport rate, expressed in a similar form as equation (5.2) is

$$q(t) = c_q wd \left\{ \frac{0.5\rho f_{cw}\left[u^2(t) + v^2(t)\right]}{(s-1)\rho g d} \right\}^3 \tag{5.5}$$

where w is the fall velocity of sediment, c_q is a constant, f_{cw} is the combined wave-current friction factor, and u and v are the velocity components that result from the combination of high-frequency (wave driven) and low-frequency (atmospheric and tide driven) currents.

A method for computing f_{cw} is given by Madsen (1987), which is essentially an iterative method that modifies the bottom boundary layer based on interaction with waves. Initially, the wave friction factor, $f_{wc,}$ for waves in the presence of currents is determined by using the equation

$$\frac{1}{4\sqrt{f_{wc}/C_\mu}} + \log\frac{1}{4\sqrt{f_{wc}/C_\mu}} = \log\frac{C_\mu u_b}{k_s \omega} - 0.17 \tag{5.6}$$

where k_s is a characteristic bottom roughness, ω is the wave radian frequency ($2\pi/T$), u_b is the magnitude of the velocity under the wave (in linear wave theory $u_b(t)=\sin[kx - \sigma t]$), and the coefficient C_μ is described as

$$C_\mu = \left(1 + 2\mu\cos\theta_c + \mu^2\right)^{1/2} \tag{5.7}$$

where

$$\mu = \left(\frac{u_{*c}}{u_{*wm}}\right)^2 \tag{5.8}$$

and θ_c is the angle between the wave approach and the current direction, u_{*c} is the current shear velocity, and u_{*wm} is the magnitude of the maximum wave shear velocity in the presence of currents. In this procedure, an initial guess for the value of μ must be made, because u_{*wm} is initially not known.

The final value of f_{cw} is computed using the equation

$$f_{cw} = 2\left(\frac{u_{*c}}{u_r}\right)^2 \tag{5.9}$$

where u_{*c} is the current shear velocity, and u_r is the magnitude of the measured current, measured at a particular height above bottom, z_r. The current shear velocity is determined by the equation

$$u_r = \frac{u_{*c}}{\kappa}\left(\ln\frac{z_r}{\delta_{cw}} + \frac{u_{*c}}{u_{*m}}\ln\frac{\delta_{cw}}{z_0}\right) \text{ ; for } z_r > \delta_{cw}\,, \tag{5.10}$$

which is quadratic in u_{*c}, and

$$u_{*wm}^2 = \frac{1}{2} f_{wc} u_b^2 , \tag{5.11}$$

$$u_{*m}^2 = C_\mu u_{*wm}^2 , \tag{5.12}$$

$$\delta_{cw} = \frac{\kappa u_{*m}}{\omega} , \tag{5.13}$$

where,

u_{*wm} = magnitude of the maximum wave shear velocity in the presence of currents,
f_{wc} = wave friction factor, for waves in the presence of currents,
u_{*m} = combined wave-current shear velocity,
δ_{cw} = wave bottom boundary layer thickness,
u_{*m} = combined wave-current shear velocity, and
κ = von Karman's constant (=0.4).

A computer program was developed using the relationships of Grant and Madsen (1986) for the purpose of computing infilling rates at a borrow site. This program uses wave model output (Section 4.0) with current data to determine bottom sediment transport potential at the perimeter of the borrow site and a resulting annualized volume rate of sediment that will enter the borrow site.

5.2.2 Model Input Data

Wave data from STWAVE model runs and ADCP current data collected offshore near Thomas Shoal provided input conditions for determining borrow site infilling rates. Wave data were extracted from the existing condition model runs at the perimeter nodes of each proposed borrow site. These are the same STWAVE model runs used to determine sediment transport potential at the coastline (see Section 4.0). Wave model input conditions used for each sand resource area are listed in Tables 5-2 through 5-5. Surface current speeds used to determine infilling rates are given in Table 5-6. These currents are based on analyses presented in Section 5.1. Currents were applied in the model based on their percent occurrence. Ambient current directions were set as alongshore and based on the direction of wave propagation for each modeled wave case.

In addition to wave and current inputs, other data and parameters were specified for each bottom transport potential model run performed for each borrow site. Depths at each perimeter node were taken from the wave model grid. Bottom sediment characteristic grain sizes (d_{90} and d_{50}) also were specified individually for each site. Parameters used for the model runs at each borrow site are listed in Table 5-7.

Table 5-2. Wave model input conditions used to compute offshore sediment transport potential for the borrow site in Area A. STWAVE model output from each modeled condition, and at each borrow site perimeter grid node, was used as input to the wave-current interaction model used to determine bottom sediment transport potential.

Wave Period Band	Peak Wave Direction, θ_p (deg true north)	H_{mo} Wave Height (m)	Mean Peak Wave Period, T_p (sec)	% Occurrence
Band 1	55	1.7	7.7	8.2
	80	1.4	7.7	20.8
	100	1.0	7.7	24.6
	130	1.5	6.3	2.3
Band 2	60	1.7	12.5	6.5
	65	1.6	12.9	28.5
	100	1.5	11.1	3.4

Table 5-3. Wave model input conditions used to compute offshore sediment transport potential for borrow sites in Area B. STWAVE model output from each modeled condition, and at each borrow site perimeter grid node, was used as input to the wave-current interaction model used to determine bottom sediment transport potential.

Wave Period Band	Peak Wave Direction, θ_p (deg true north)	H_{mo} Wave Height (m)	Mean Peak Wave Period, T_p (sec)	% Occurrence
Band 1	25	1.9	6.9	2.3
	45	1.8	7.6	6.5
	65	1.6	7.7	14.2
	90	1.1	7.7	24.7
	105	1.1	6.9	5.7
Band 2	50	1.7	11.4	6.7
	65	1.7	13.9	24.1
	90	1.7	13.4	6.6

Table 5-4. Wave model input conditions used to compute offshore sediment transport potential for borrow sites in Area C. STWAVE model output from each modeled condition, and at each borrow site perimeter grid node, was used as input to the wave-current interaction model used to determine bottom sediment transport potential.

Wave Period Band	Peak Wave Direction, θ_p (deg true north)	H_{mo} Wave Height (m)	Mean Peak Wave Period, T_p (sec)	% Occurrence
Band 1	32	1.6	6.8	4.5
	47	1.5	7.5	12.3
	72	1.3	7.5	15.6
	87	1.0	6.9	11.5
	107	1.1	5.4	4.5
Band 2	52	1.4	12.3	18.4
	62	1.5	13.3	19.4
	87	1.1	11.1	2.0

Table 5-5. Wave model input conditions used to compute offshore sediment transport potential for borrow sites in Area D. STWAVE model output from each modeled condition, and at each borrow site perimeter grid node, was used as input to the wave-current interaction model used to determine bottom sediment transport potential.

Wave Period Band	Peak Wave Direction, θ_p (deg true north)	H_{mo} Wave Height (m)	Mean Peak Wave Period, T_p (sec)	% Occurrence
Band 1	50	1.4	6.9	7.0
	65	1.3	7.4	15.3
	90	1.2	6.9	14.1
	110	1.2	5.5	5.9
	135	1.1	4.9	4.1
Band 2	75	1.3	12.9	24.5
	80	1.3	13.0	12.6

Table 5-6. Surface current speeds used to compute offshore sediment transport potential based on the analyses in Section 5.1.

Current Speed (cm/sec)	Exceedence Occurrence (%)
54	0.1
39	2
32	5
25	10
16	25
12	50

Table 5-7. Borrow site characteristic depths and bottom sediment grain sizes used as bottom sediment transport potential model input.

Borrow Site	Average Bottom Depth (m)	Sediment Size, d_{10} (mm)	Sediment Size, d_{50} (mm)
A1	10.6	0.70	0.32
B1	13.9	1.15	0.60
B2	12.2	1.49	0.47
C1 north	13.0	1.96	0.61
C1 south	12.9	0.62	0.29
D2	18.7	0.50	0.31

5.2.3 Infilling Model Results

Infilling rates computed for six central east Florida borrow sites represent the total potential transport magnitude into each of the sites (Table 5-8). These results likely represent an upper bound for sediment transport at each site, assuming linear wave dynamics and an unlimited sediment supply. Of the six modeled borrow sites, Site A1 has the greatest infilling rate as a result of a combination of factors, including its shallow depth relative to other sites and its large perimeter. Because the borrow site is in relatively shallow water, wave-induced currents and wind-driven currents are large, and more sediment can

be mobilized in the proximity of the borrow site. Sites that have a larger perimeter generally will trap more sediment over a given period. Furthermore, sediment grain size also affects sediment mobility, such that relatively smaller gain sizes at Site A1 would tend to be more mobile than larger sediment identified at other areas.

Table 5-8. Characteristic dimensions, computed borrow site infilling rates, and estimated time to fill based on total proposed excavated volume.

Borrow Site	Borrow Site Area (m^2)	Excavated Volume ($x\ 10^6\ m^3$)	Average Depth (m)	Infilling Rate (m^3/yr)	Infilling Time (yr)
A1	$5.4x10^6$	13.6	10.6	538,000	25
B1	$4.6x10^6$	11.0	13.9	152,000	141
B2	$3.5x10^6$	7.6	12.2	407,000	54
C1 north	$5.2x10^6$	5.8	13.0	152,000	73
C1 south	$4.7x10^6$	8.8	12.9	98,000	122
D2	$2.2x10^6$	4.1	18.7	5,000	770

Total infilling times presented in the last column of Table 5-8 were computed using the total design excavated volume divided by computed infilling rates. As such, they represent the length of time required to fill a site that is excavated to the total design depth during a single dredging event. Site D2 has the longest total infilling time, resulting primarily from the small infilling rate computed for this area and large average water depth. Site A1 has the shortest infilling time due primarily to its large computed infilling rate and shallow depth. These estimated infilling times are most useful as a relative guide for borrow site infilling rather than an absolute indicator of exactly how long it takes for the borrow site to fill.